ROYAL SOCIETY OF CHEMISTRY

Journal Name

ARTICLE

Received 00th January 20xx, Accepted 00th January 20xx

DOI: 10.1039/x0xx00000x

www.rsc.org/

Surface directed reversible imidazole ligation to nickel(II) octaethylporphyrin at the solution/solid interface: A single molecule level study†

Goutam Nandi, ^a Bhaskar Chilukuri, ^a K. W. Hipps, *^a and Ursula Mazur*^a

Scanning tunneling microscopy (STM) is used to study for the first time the reversible binding of imidazole (Im) and nickel(II) octaethylporphyrin (NiOEP) supported on highly oriented pyrolytic graphite (HOPG) at the phenyloctane/NiOEP/HOPG interface at 25 °C. The ligation of Im to the NiOEP receptor while not observed in fluid solution is readily realized at the solution/HOPG interface. The coordination process scales with increasing Im concentration and can be effectively modeled by the Langmuir isotherm. At room temperature it is determined that the standard free energy of adsorption is $\Delta G_c = -15.8$ kJ/mole and the standard enthalpy of adsorption is estimated to be $\Delta H_c \approx -80$ kJ/mole. The reactivity of imidazole toward NiOEP adsorbed on HOPG is attributed to charge donation from the graphite stabilizing the Im-Ni bond. This charge transfer pathway is supported by molecular and periodic modeling calculations which indicate that the Im ligand behaves as a π -acceptor. DFT calculations also show that the nickel ion in the Im-NiOEP/HOPG complex is in a singlet ground state. This is surprising since both our calcualtions and previous experimental studies find a triplet ground state for the five and six coordinated Im-nickel (II) porphyrins in the gas-phase or in solution. Both the experimental and the theoretical findings provide information that is useful for better understanding of chemical sensing/recognition and catalytic processes that utilize metal-organic complexes adsorbed on surfaces where the reactivity of the metal is moderated by the substrate.

Introduction

Coordination chemistry of metalloporphyrins plays an essential role in many enzymatic catalytic functions, ¹ electron and energy transfer, and sensing (molecular recognition). ² Enzymes reversibly bind to their substrates as part of their catalytic cycles. ³ Cytochromes transfer electrons ⁴ while myoglobin and hemoglobin transport and store oxygen. ⁵ The multiple porphyrinic binding sites in the biological systems are unsurpassed in their function as receptors that can regulate ligand binding events. Duplication of this behavior in artificial metalloporphyrin systems is of tremendous interest for the purpose of separating gas mixtures, ⁶ energy storage and delivery, selective chemical sensing, ² and basic understanding of kinetics and thermodynamics of catalysis.

Metalloporphyrin systems adsorbed on solid surfaces (where they readily form ordered monolayers by self-assembly) provide models for molecular recognition studies that imitate the porphyrin receptors in biological systems. Advantageously, pertinent thermodynamic and kinetic parameters for chemical

processes at the solid/solution interface. 13,14

surface processes also lend themselves to be studied at a

molecule level using scanning tunneling microscopy (STM).⁷

The vast majority of STM studies of axial coordination to metal porphyrins to date, were performed at the solid/vacuum interface and have been summarized in an excellent review article by Gottfried.¹¹ These reactions involved small molecules such as NO, CO, and NH₃ binding to d⁵ – d¹⁰ transition metal substituted porphyrins absorbed on crystalline metal substrates (Au, Ag, Cu, etc.) and HOPG. By comparison there are only a handful of reports on ligand binding chemistry at the solution/solid interface (none of them with Ni as a central metal) and almost no quantitative kinetic or thermodynamic studies

¹¹ STM is the ideal tool for investigating ligand binding events because of its submolecular resolution, sensitivity to electronic structure, and the ability to function in vacuum, air, and at the solution/solid interface, an environment most relevant to solution based biological and chemical processes.^{8, 12} Furthermore, by varying the pressure or concentration of reagents as well as the reaction temperature, one can extract

^a- Department of Chemistry and Materials Science and Engineering Program, Washington State University, Pullman, Washington 99164-4630. E-mail: <u>umazur@wsu.edu</u>, <u>hipps@wsu.edu</u>.

[†]Electronic Supplementary Information (ESI) available. ESI contains an additional STM image of Im-NiOEP. It has details about molecular DFT calculations, periodic plane-wave (PW) DFT calculations, charge density and integration as a function of distance, density of states, and calculation of the entropy of binding/adsorption. See DOI: 10.1039/x0xx00000x

A few articles have reported surface observation of complexes that are also known to form in solution. Stable fivecoordinated zinc porphyrin - nitrogen base complexes were adsorbed at the solution/solid interface from organic solvents containing mixtures of metalloporphyrin and a ligand (no kinetic or thermodynamic studies were conducted). 15-17 Feringa¹⁵ imaged Zn tetradodecylporphyrin axially coordinated to 3-nitropyridine at the tetradecane/ HOPG interface while Otsuki¹⁶ observed both cis and trans-phenylazopyridine Zn octadecyloxyphenyl porphyrin complexes on HOPG in phenyloctane solution.¹⁷ The formation of different manganese oxo species was proposed by De Feyter et al. for the reaction of oxygen and the metalloporphyrin adsorbed at the octanoic acid/Au(111) interface. 10 While oxygen binding to this manganese porphyrin can occur in solution, they also observed processes occurring at adjacent sites on the surface. In all of the above reports, the metal porphyrin-ligand complexes imaged at the solution solid interface can be readily formed in solution, thus it is unclear what role, if any, the substrate played in their formation.

A rare example of complexation occurring exclusively with a surface supported species was given by Friesen and coworkers.

They conducted temperature dependent STM measurements of O₂ reversible binding to cobalt(II) octaethylporphyrin (CoOEP) at the phenyloctane/HOPG interface and provided detailed insight into the kinetics and thermodynamics of the ligation.

Interestingly, in some of the above mentioned reactions, the supporting surface acted in a manner similar to an electron-donating ligand bound to the fifth coordination site of the coordinating metal, thereby greatly influencing the receptor ability of the metal porphyrin adsorbate. Such was true for cobalt ion in Co octaethylporphyrin (CoOEP) adsorbed on HOPG and its increased affinity for oxygen binding which was attributed to charge donation from the surface to the Co(II) ion.¹³

There is a great need for quantitative STM studies investigating the kinetics and the thermodynamics of ligand binding to metalloporphyrins at the solution/solid interface in order to provide new insights into the structural and electronic factors which stabilize the metal ion – ligand bond. Such studies also will yield an improved understanding of the donor-acceptor properties in metal porhyrin-ligand complexes.

Here we report the thermodynamics of imidazole (Im) ligation to nickel (II) octaethyl-porphyrin (NiOEP), Fig. 1, supported on HOPG at the phenyloctane/NiOEP/HOPG interface using STM imaging. Synthetic nickel porphyrins have been extensively used as model systems for investigating the dynamics of binding of basic ligands, because, unlike cobalt and iron, nickel ion does not bind exogenous ligands such as CO and O₂. ¹⁸⁻²³ In myoglobin and hemoglobin an imidazole coordinated opposite to O₂ is required for oxygen to bind to the iron centers. ^{19,24} In solution, five-coordinated nickel porphyrin intermediates are rarely observed. ²² However, six-coordinated adducts with two axial ligands are common. ^{3,5,18,20} The degree to which two nitrogen bases coordinated to the metal center is controlled by the Lewis basicity of the ligand and the acidity of

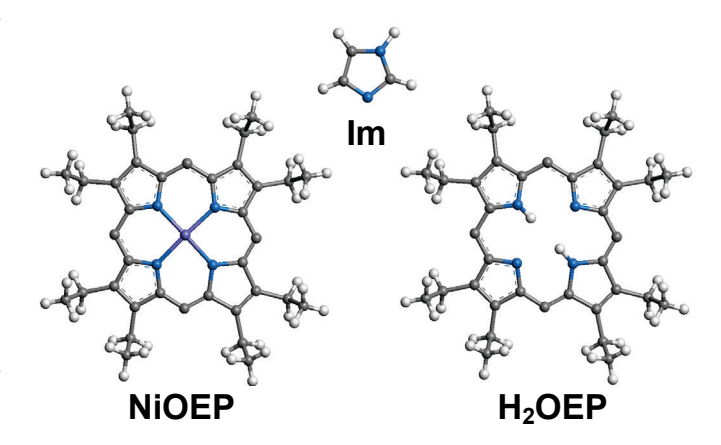


Fig. 1 Molecular models of imidazole (Im), $\,$ nickel octaethylporphyrin (NiOEP), and free-base octaethylporphyrin ($\,$ H₂OEP). The porphyrins are with the ethyl groups up configuration. Gray atoms are carbons, white are hydrogens, blue are nitrogens, and purple is nickel.

the nickel ion which, in turn, is modulated by the electron donating and withdrawing capability of the substituents on the periphery of the macrocycle. Because imidazole is a weak Lewis base (pKa = 6.65^{25}), the nickel porphyrin receptor needs to be sufficiently electron deficient to support axial binding of the ligand. The reported equilibrium binding constants for six coordinated Im-Ni tetrapyrrole complexes are comparatively small. For example, the equilibrium constants for monoligation (K_1) and biligation (K_2) for species formed with imidazole and nickel meso-tetramethylpyridyl porphyrin (NiTMPyP) in water acetone solution at 25°C were 8.39 M⁻¹ and 0.19 M⁻¹, respectively. 26 For the Im and Ni-bacteriochlorophyll-a (Ni-BChl) binding reaction in acetonitrile $K_1 = 29.6 \pm 1.1 \text{ M}^{-1}$ and $K_2=26.8\pm0.9$ M⁻¹, correspondingly. ¹⁸ In the absence of strong electron withdrawing substituents on the macrocycle, nickel porphyrin complexes essentially show no tendency to bind imidazole in solution, e.g.; nickel tetraphenyl porphyrin, NiTPP. 23 Similarly NiOEP is not expected to bind Im. In what follows we verify that NiOEP does not bind imidazole in solution but it does coordinated to the porphyrin adsorbate at the solution/HOPG interface. Furthermore, we show that the binding reaction is reversible and can be readily monitored by sequential STM imaging. The Im ligation to NiOEP receptors on the HOPG surface correlates directly with increasing Im solution concentration. This process can be satisfactorily described by the Langmuir adsorption model. Relevant thermodynamic parameters are extracted from this isotherm.

To complement the experimental ligation studies we carried out DFT calculations in order to better understand the structural and electronic character of NiOEP during the Im ligation/deligation processes at the solution/solid interface. It is generally accepted that in solution the nitrogen ligands (one or two) sufficiently destabilize the d_{z2} Ni orbital in the singlet state (denoted here as S_0) of a tetrapyrrole complex that an electron is promoted to the d_{x2-y2} orbital, resulting in metal ground state having a d_{z2} , d_{x2-y2} configuration. Thus, the solution phase complex is expected to be in a triplet state, denoted here as T_1 .²² On the graphite surface we are, in effect, forming a five coordinated Im-NiOEP species (stabilized by the substrate) which, by extension, should be a high spin complex. Our

molecular modeling calculations, however, predict a different electronic character for the surface bound Im-NiOEP adduct than the expected triplet state found for the same molecular system in solution or in the gas phase. This surprising result is addressed in the context of the charge allocation in the imidazole coordinated NiOEP complex formed in different chemical environments. Calculations also indicate that the HOPG substrate donates charge to the NiOEP adsorbate which in turn donates charge to the imidazole ligand. In this scenario, Im acts as $\pi\text{-acceptor}$, a role which is different from what is reported about imidazole binding to Ni porphyrins in solution. 3,5,18,20 In a liquid environment the porphyrin receptors need to be sufficiently electron deficient to support axial binding of the Im ligand. 23

Experimental section

Materials

2,3,7,8,12,13,17,18-octaethyl-21H,23H-porphine nickel(II), NiOEP, and 2,3,7,8,12,13,17,18-octaethyl-21H,23H-porphine, H₂OEP, were purchased from PorphyChem without further purification. Imidazole, 99% pure, was acquired from Alfa Aesar. Reagent grade toluene was purchased from J.T. Baker. Phenyloctane (99%) was purchased from Alfa Aesar and was distilled over Al₂O₃ before use.²⁷ Highly ordered pyrolytic graphite (HOPG) substrates (Grade 2, a 1 cm² size) were purchased from SPI Supplies and freshly cleaved before use.

STM Imaging

STM images were recorded using a Molecular Imaging (now Keysite Technology) Pico 5 STM equipped with a 1µm² scanner. The sample and scanner are enclosed in an isolation chamber that was held under ambient air or argon environment. STM tips were made by cutting or electrochemically etching Pt_{0.8}Ir_{0.2} wire (California Fine Wire Company). Images were typically obtained at a sample potential of 0.2-0.5 V and a tunneling current of 30-20 pA. Typical scan rates were 4.7 lines/sec, giving a total image time of 2.0 min. No drift correction was applied. All images were background subtracted using SPIPTM image processing software. ²⁸

Solutions of NiOEP and H₂OEP were prepared by dissolving solid porphyrin compounds in phenyloctane. Concentrations were measured using an UV-vis spectrophotometer where the extinction coefficient of each species had been previously measured by applying Beer's law to a series of dilutions of a known concentration solution. 27 Stock solutions of 6.79×10^{-5} M NiOEP and 8.52×10^{-5} M H₂OEP were prepared separately and used to prepare a 9:1 and 7.5:2.5 molar mixtures of NiOEP:H₂OEP in phenyloctane with average concentrations 6.96×10^{-5} M and 7.22×10^{-5} M, respectively. Imidazole solutions in *n*-octylbenzene (phenyloctane) ranged from 2×10^{-1} 4 to 1.5×10^{-3} M. The same stock solutions of the porphyrins and Im were used for all of the experiments performed by STM. The use of 10% inert porphyrin is discussed in the Supporting Information section A. Typically, a 10 µL aliquot of porphyrin solution was placed onto HOPG followed by the addition of 10

 μL of imidazole solution of desired concentration. A custom-made solution cell sample holder was used to accommodate the solution in contact with the substrate surface.

Electronic Spectra

UV-visible studies were carried out using a Thermo Scientific Evolution 260 Bio spectrophotometer with 0.1578 cm path length cuvettes. UV-visible spectroscopy on saturated and filtered solutions of porphyrins in toluene was used to determine solubility at room temperature.²⁷

Computational section

Molecular Modelling

The Gaussian 09 package²⁹ was used to perform density functional theory (DFT) calculations. Simulations were carried out with the B3LYP^{30,31,32} hybrid functional in conjunction with 6-311++G(d,p) basis set³³ for all optimization and single point calculations. All simulations were performed in gas phase and in solution phases using the SMD³⁴ implicit solvation model with benzene as solvent. The charge population was obtained using natural bond orbitals (NBO).^{35,36}

Periodic Modeling Methodology

Simulations were performed using the Vienna Ab initio Simulation Package (VASP)^{37,38,39} version 5.2. Periodic calculations were performed using plane-wave density functional theory (PW-DFT) within the projector augmented wave (PAW) method^{40, 41} to describe the core electrons and valence-core interactions. The computations were performed with B3LYP^{31, 32} and HSE⁴² hybrid functionals and with PBE⁴³ and B88⁴⁴ non-hybrid functionals. PAW-PBE potentials having p, s semicore valence were used for the Ni atom. It was previously reported 45,46 that calculations of organic species on surfaces with dispersion corrections yields better geometries and predicts more accurate binding energies. Hence, we used the vdW-DF method, 47-49 which takes into account the nonlocal nature of electron correlation in conjunction with all the aforementioned DFT functionals, for all our calculations. For slab calculations, the electronic wave functions were sampled in a k-point grid of $2\times2\times1$ in the irreducible Brillouin zone (BZ) using the Monkhorst and Pack (MP)⁵⁰ method. Isolated molecules were sampled with the gamma point. A plane wave cut off energy of 550 eV was used for all simulations and this value is determined from energy convergence tests on HOPG primitive lattices. Methfessel-Paxton smearing was used to set the partial occupancies for each wave function with a smearing width of 0.2 eV.

Results and discussion

Fig. 1 shows the molecular structures of NiOEP, H₂OEP, and imidazole (Im). When adsorbed on a surface the alkyl groups on the macrocycles are in an all up orientation as was established by

previous STM studies of the octaethylporphyrins adsorbed on HOPG 8,51,52,53,54 and Au(111). 8,27

As discussed before, NiOEP is not expected to bind imidazole in solution at room temperature. To confirm this, UV-vis spectra of pure nickel octaethylporphyrin and NiOEP in a great excess of Im in toluene were obtained after a 24 hour reaction time. Fig. 2 reveals that a 50 fold molar excess of Im to NiOEP in toluene solution produces no change in either the Soret or Q bands, indicating that no imidazole porphyrin complex is formed. In chloroform where the imidazole is much more soluble, ratios of 1000 to one of Im to NiOEP leave the NiOEP spectrum unchanged. This lack of reactivity between Im and NiOEP is further supported by molecular DFT calculations (Supporting Information B) which confirm that imidazole will not bind to NiOEP molecule with nickel in the singlet (S₀) spin state. (Note that both isolated imidazole and NiOEP molecules exist as singlets in their ground state.) However, calculations do support a hypothetical five-coordinated Im-NiOEP intermediate with the nickel ion in a triplet (T₁) ground state. Such a complex would have characteristic dome shaped geometry (Fig. SI-4a, 4b) similar to the structures of Ni porphyrins ligated to a single base as reported by Shellnutt and coworkers.²² Our DFT findings about the conversion of spin structure are also consistent with similar calculations reported on Ni porphyrins with other nitrogenous bases.55

In addition to calculating the electronic state of the Ni ion in a five-coordinated Im-NiOEP system, molecular DFT calculations were also performed on the six coordinated NiOEP adduct with two axial imidazole ligands. As in the case with 5-coordinated complex, Im-NiOEP (Fig. SI-4a, 4b), the 6-coordinated complex, Im-NiOEP-Im (Fig. SI-4c, 4d) complexation is also only possible in the triplet (T₁) spin state. Resonance Raman spectra⁵⁶ showed that Ni(II) porphyrins are always high spin when bound to nitrogenous bases via the 5th or 6th coordination site. In the Im-NiOEP-Im complex, the porphyrin core has a flat geometry contrary to the dome structure seen in Im-NiOEP complex. The Mulliken spin density of both 5 and

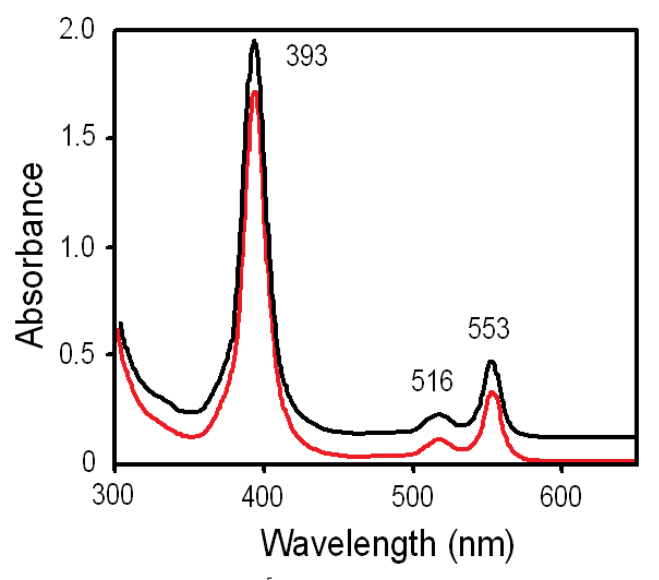


Fig. 2 UV-vis spectra of 1.2×10^{-5} M NiOEP in toluene solution (black trace) and 1.2×10^{-5} M NiOEP and 6.0×10^{-4} M imidazole in toluene (red trace). The spectral data are offset for easier comparison.

6 coordinated high-spin (T_1) Im-NiOEP complexes reveal large spin localization on the Ni atom (~ 1.5 e $^{-}$) and porphyrin nitrogens (~ 0.4 e $^{-}$) with negligible spin density on the rest of the atoms. Molecular DFT calculations also indicated that imidazole binds to NiOEP (in triplet state) with an adsorption energy of ~ -20 kJ/mol in the gasphase and ~ -13 kJ/mol in the solution (benzene). Whether in an optimized triplet or frozen singlet (at triplet geometry) of the 5-coordinated Im-NiOEP complex, it was found that imidazole donates charge of ~ 0.2 e $^{-}$ and ~ 0.1 e $^{-}$ to the NiOEP molecule respectively. This charge transfer is consistent with the reported gas-phase based DFT calculations on a Ni–BChl (bacteriochlorophyll) imidazole complex which suggested that the porphyrin core was enriched by 0.21 electron charge units upon ligation to a single imidazole molecule. 57,58

While the DFT calculations indicate a negative binding energy, it is the free energy that determines the stability of the Im-NiOEP complex. Using methods first discussed by Whitesides, ⁵⁹ we have estimated the entropy of complexation of Im with NiOEP in phenyloctane (see Supplemental Information, Section F). We find that $\Delta S \approx 216$ J/mole-K. In condensed phase the difference between ΔE and ΔH is small, so using the DFT value of -13 kJ/mole as ΔH_{sol} , the free energy of binding in solution (as T_1) at 298K, ΔG_{sol} , is about

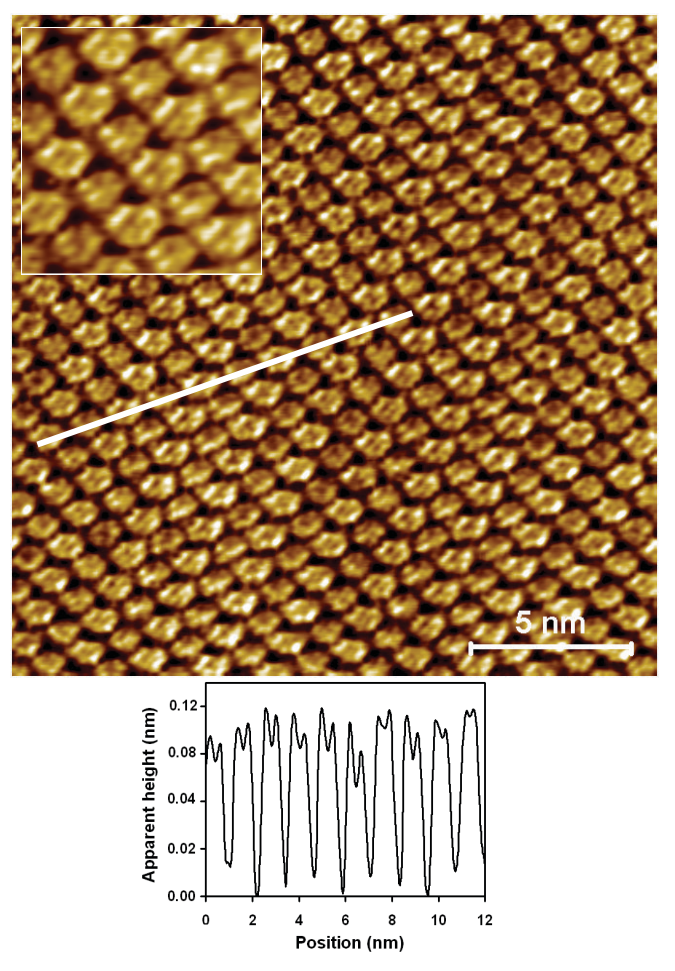


Fig. 3 Constant current STM image of 9 NiOEP:1 H₂OEP/HOPG surface in phenyloctane acquired at 20 pA set point and 600mV bias. The 5 nm² inset shows submolecular resolution of the porphyrin molecules. The cross sectional profile emphasizes the lack of distinction between the two different porphyrins.

+51 kJ/mole or an equilibrium constant of 1x10⁻¹¹. Only at extremely low temperatures might observation of this reaction be possible.

UV-Vis spectra and molecular DFT calculations confirm that imidazole does not bind to NiOEP in solution/gas-phase near room temperature. The binding of Im to NiOEP adsorbed on a surface was investigated next.

To follow the kinetics of imidazole ligation to NiOEP at the solution/HOPG interface we employed pure NiOEP dissolved in phenyloctane and NiOEP solutions (in phenyloctane) containing a small amount H₂OEP used as an internal reference. In the absence of a metal ion, the Im is not expected to coordinated to the porphyrin molecule. The free-base reference molecules aided in optimizing the contrast in the images of the ligated and unligated nickel ions for a

more accurate total count of the complexed molecules, especially when low Im concentrations (10^{-4} M) were used (see supplementary information section A for more details).

Fig. 3 presents a STM image of the monolayer formed from a solution of NiOEP and H₂OEP in a 9:1 molar concentration ratio in phenyloctane. Both porphyrin molecules are expected to have a depression in the center of the macrocycle based on previous UHV^{51,60}and solution studies of the nickel and free-base tetrapyrrole^{11,27,53} compounds. As can be seen from both the image and the cross sectional profile (Fig. 3), NiOEP cannot be distinguished from H₂OEP. In the 5 nm² inset, the submolecular features are the ethyl groups extending from the periphery of the porphyrin rings. It is gratifying that the high resolution images of MOEP acquired in solution on HOPG can approach (but not attain)

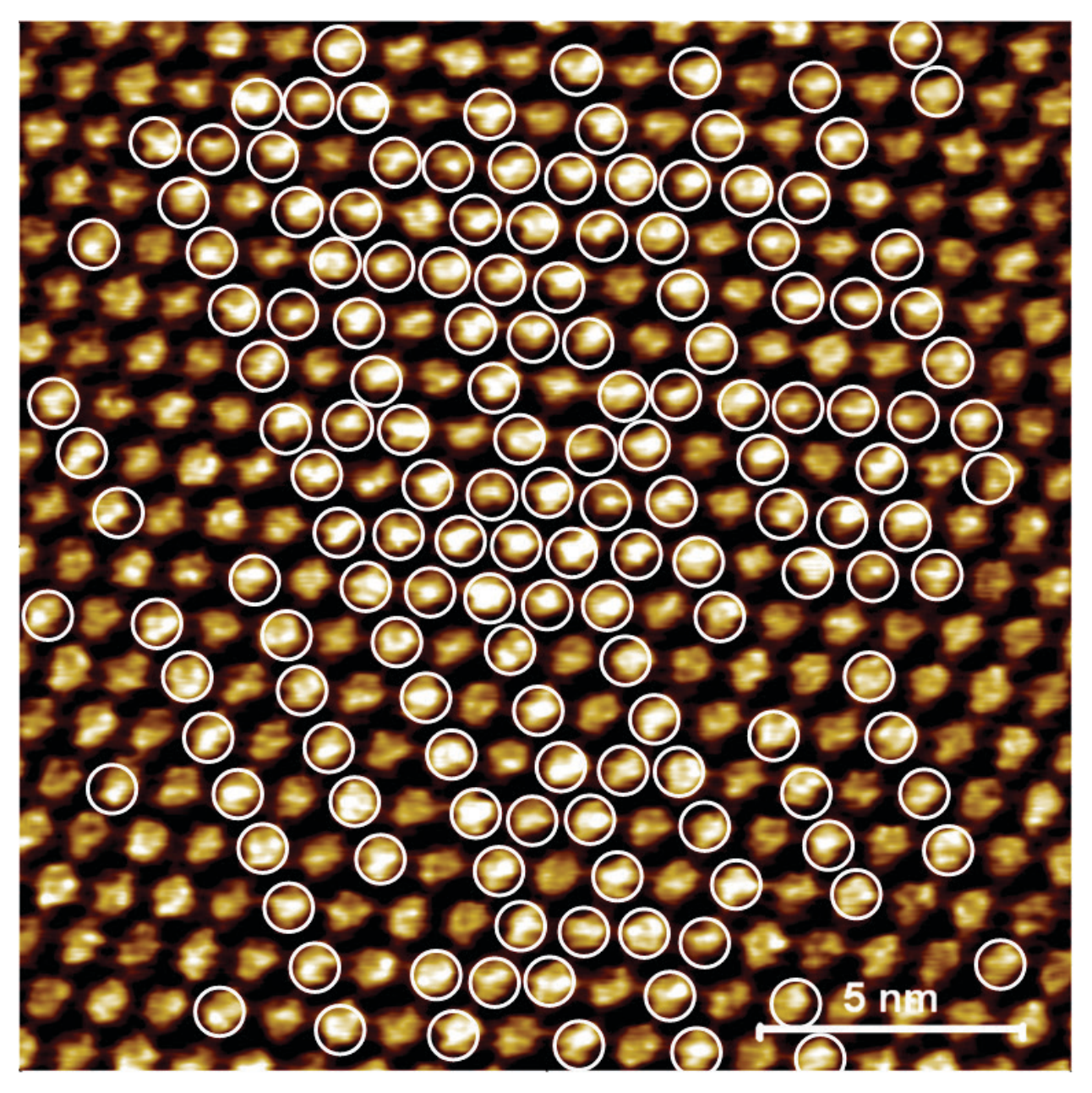


Fig. 4 Constant current STM image of the phenyloctane/NiOEP/HOPG interface with approximately 50% of the NiOEP surface adsorbate ligated to Im at 25 °C. Data was acquired at 0.2 V and 50 pA set point. Note that the molecules enclosed in circles are brighter than others and denote the Im-NiOEP ligated complexes.

the resolution observed in UHV images of NiOEP on $Au(111)^{51}$ and H_2OEP on $Ag(111)^{.60}$

Although one cannot differentiate the NiOEP and H₂OEP in the image (Fig. 3) either visually or by examining their cross sectional profile, the relative amounts of each porphyrin present in the monolayer are expected to mirror their respective mole fraction concentrations in solution. Bhattarai and coworkers studied the adsorption of mixtures of CoOEP and NiOEP at the solution/solid interface and concluded that these porphyrins adsorbed very strongly on both HOPG and Au(111) surfaces and retained the same monolayer composition as their solution concentrations.^{27,54} Furthermore, these mixed porphyrins layers were stable at room temperature and required heating to 70 °C and 100 °C to initiate their desorption from HOPG and Au(111) surfaces, respectively.

Upon addition of the imidazole ligand solution to the phenyloctane/NiOEP/HOPG system one could (after a short time) observe even at low imaging resolution that the surface was now covered with both bright and dim molecules (Fig. 4). The bright molecules are the Im-NiOEP/HOPG adducts while the dim molecules are the unreacted NiOEP/HOPG and 10% reference $\rm H_2OEP/HOPG$. We interpret these new bright centers as resulting from charge transfer to the imidazole upon surface complexation. Calculations (discussed later) support this view of net electron transfer from HOPG to the imidazole. Friesen et. al. have shown previously that HOPG can act in a manner similar to an electron-donating ligand bound to the fifth coordination site on the cobalt ion of CoOEP, thereby greatly increasing the compound's affinity for oxygen. 13

To better understand the nature of the binding of imidazole to NiOEP adsorbed on the HOPG substrate, PW-DFT calculations are performed. The experimental evidence that NiOEP does not coordinated imidazole in solution or in gas phase, but does so at the NiOEP/HOPG interface prompted us to examine the electronic and spin structure of Im-NiOEP complex on HOPG in some detail. We performed spin-polarized PW-DFT calculations on the isolated Im, NiOEP, Im-NiOEP molecules and on the HOPG, NiOEP/HOPG and Im-NiOEP/HOPG periodic slab structures. Specifics of the simulation models are presented in the Supporting Information section C. Periodic DFT calculations with various functionals (vide supra) on isolated Im, NiOEP, Im-NiOEP molecules are generally consistent with our molecular DFT calculations. For similar simulation comparison, all the results presented here are obtained using B3LYP functional unless mentioned otherwise. In both molecular and periodic simulations Im and NiOEP molecules are singlets (S₀) in their ground states. Furthermore, Im prefers to coordinated to the Ni⁺² in NiOEP in a triplet spin state because Im-NiOEP high spin (T_1) complex (five or six-coordinated) has a lower energy than the low spin (S₀) system (Table SI-2). Also, the characteristic dome structure is predicted in the high spin fivecoordinated Im-NiOEP adduct. Additionally, the valence charge redistribution obtained using Bader charge analysis, ⁶¹ for the isolated Im-NiOEP high spin complex indicates a charge transfer of ~0.2 e⁻ from imidazole to NiOEP which is also consistent with molecular DFT calculations (*vide supra*). This is not the situation for the HOPG supported system.

PW-DFT simulations on HOPG, NiOEP/HOPG, Im-NiOEP/HOPG slab structures indicate that all of these have a lower S_0 energy than the T_1 spin state (Table SI-2). Whether NiOEP is an isolated molecule or adsorbed on HOPG substrate, $S_0 \le T_1$ by ~45 kJ/mol. However, in an isolated Im-NiOEP complex, $T_1 \le S_0$ by ~ 30 kJ/mol. On the contrary, if Im-NiOEP is adsorbed on HOPG, $S_0 \le T_1$ in energy by ~ 20 kJ/mol. The energy difference between S_0 and T_1 in the Im-NiOEP/HOPG system is very little (~ 20 kJ/mol). So to confirm this difference, we performed PW-DFT calculations (with optimization) on So and T1 structures of Im-NiOEP/HOPG system with another hybrid HSE functional⁴² with the same potentials used with B3LYP functional. Results obtained using the HSE functional also yielded a similar trend showing that $S_0 < T_1$ in Im-NiOEP/HOPG system by ~23 kJ/mole. Hence, we propose that Imidazole binds to NiOEP on HOPG in a singlet ground state which is not possible when NiOEP is the gas-phase or in solution. We believe that HOPG substrate is aiding the binding of Im ligand to NiOEP by acting as a donor of charge. This assumption can be further justified by examining the charge distribution at the Im-NiOEP/HOPG interface (vide infra).

Calculated binding energies of imidazole to NiOEP/HOPG in vacuum for the S_0 ground state depend somewhat on functional used. Values range from a high of -65 kJ/mole (PBE) through -56 kJ/mole (HSE), to a low of -34 kJ/mole (B3LYP). These adsorption energies indicate that imidazole binding to NiOEP is more favorable when NiOEP is on the HOPG surface than when it is isolated. However PW-DFT calculations under estimate the adsorption energy of Im on NiOEP/HOPG in phenyloctane as estimated from our STM experiments (*vide infra*) where $\Delta H \approx -80$ kJ/mol. This difference can be attributed, in part, to the solvation, wetting and de-wetting energies that come into effect at the solution-solid interface 62 but not considered in a gas-phase calculation. Also, given the dependence on functional of the calculated binding energy, an error of 0.2 to 0.3 eV in the calculated binding energy is quite possible.

The charge redistribution at the Im-NiOEP/HOPG interface can be obtained by taking the charge density (CD) difference at the interface using Poisson's equation similar to previous studies. 46,63 In Fig. 5, the CD-difference mappings were plot using the following equations:

$$\rho_{diff} = \rho_{PH} - \rho_P - \rho_H$$

$$\rho'_{diff} = \rho_{IPH} - \rho_I - \rho_{PH}$$

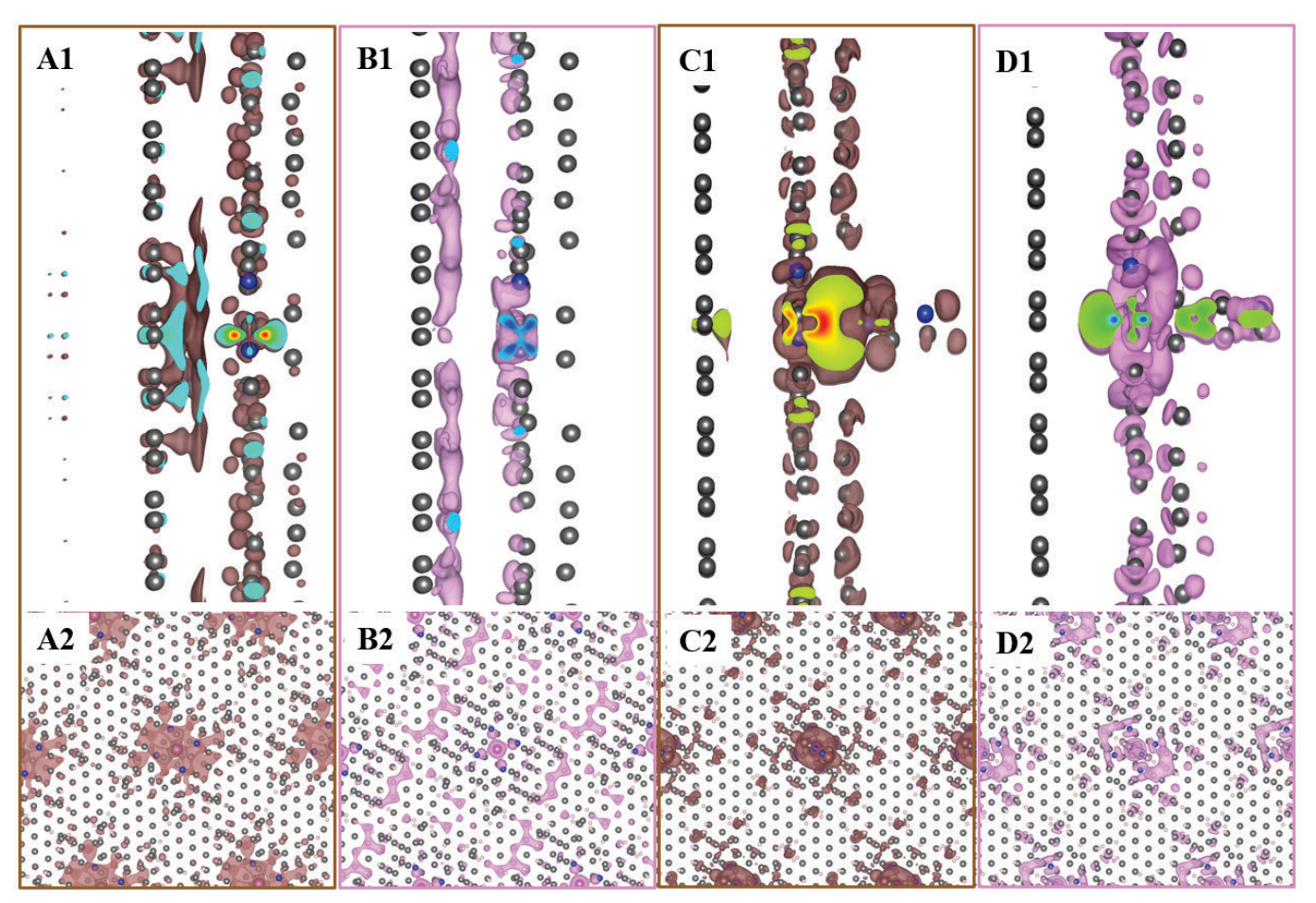


Fig. 5 Form left to right, charge density difference mappings for positive (colored in brown) and negative (colored in pink) charges for NiOEP/HOPG (A, B) and Im-NiOEP/HOPG (C,D) systems respectively. The images in the top row (A1-D1) represent side-view (along the a-axis) and the bottom row (A2-D2) represent top-view (along c-axis). Element colors are carbon-gray, nitrogen-blue, nickel-yellow (not visible). Hydrogens are masked for clarity. In the cross-section (A1-D1, top row) the rainbow colors (blue to red) indicate charge with blue being highly negative and red being highly positive.

Here, ρ_{diff} and ρ'_{diff} represents the CD-difference at the NiOEP/HOPG and Im-NiOEP/HOPG interfaces respectively. PIPH, ρ_{PH} , ρ_{I} , ρ_{P} , ρ_{H} represents the total 3-dimensional valence charge densities of Im-NiOEP/HOPG, NiOEP/HOPG, Im, NiOEP and HOPG systems obtained from individual single point energy calculations (using geometries from Im-NiOEP/HOPG interface) of each component respectively. Note that the net total charge (sum of positive and negative charges) on each system would be zero. If we could obtain the positive and negative charges as a function of position along the c-axis of the lattice, and integrate the charges we could predict whether HOPG is acting as a donor or acceptor of electronic charge to the monolayer (NiOEP or Im-NiOEP). More details on charge redistribution and integration of charge as a function of position along the c-axis of the lattice in each system is presented in the Supporting Information, section D (Fig. SI-6, Tables SI-3, SI-4).

Examining Fig. 5 one can see that, for NiOEP/HOPG interface, positive charge (Fig. 5A) is mostly located on NiOEP monolayer and its vicinity, while negative charge (Fig. 5B) is located on the HOPG substrate. But with the presence of imidazole, in Im-NiOEP/HOPG interface, the positive charge (Fig. 5C) is reduced on the Im-NiOEP monolayer in comparison to negative charge (Fig. 5D). On HOPG substrate there is almost no negative charge (Fig. 5D) but very little

positive charge (Fig. 5C) at the iso-value of 0.0003. To obtain quantitative data on charge redistribution, we integrated the positive and negative charges above and below the interface between monolayer (NiOEP or Im-NiOEP) and HOPG substrate (see Tables SI-3, Fig. SI-6 in Supporting Information for details). It was found that at the NiOEP/HOPG interface, HOPG gains a charge of ~0.1 e from each NiOEP molecule; but, in the Im-NiOEP/HOPG case, HOPG donates charge of ~0.4 e to each Im-NiOEP complex. In other words, HOPG acts as an acceptor of electronic charge from NiOEP without imidazole but as a donor in the presence of imidazole bound to NiOEP.

Further assessment of charge distribution (Table SI-4, Fig.-SI-6) in the Im-NiOEP/HOPG interface indicates that the charge donated by HOPG (~0.4 e) to Im-NiOEP complex is shared only a little on NiOEP (~0.1 e) and mostly on imidazole (~0.3 e) ligand. This is an unexpected finding because imidazole is assumed to be primarily a two electron donating ligand. But, when Im binds to NiOEP on HOPG, it acts as a charge acceptor. To verify if imidazole can retain negative charge as a molecule, we performed molecular DFT calculations on neutral and anionic imidazole molecules. Optimizations of both (anion and neutral) molecules yielded no imaginary frequencies as confirmed by calculation of the energy Hessian. The calculations also indicate that the negative charges on

the neutral and anionic Im molecules, obtained with natural population analysis (NPA),³⁶ are mostly on the nitrogens. The natural charges on neutral and anion Im are depicted in Fig. SI-7. Interestingly, the positive and negative charge redistribution (Fig. SI-9) in the Im-NiOEP/HOPG system is similar to that observed for charge difference between imidazole anion and neutral molecules (Fig. SI-8). The charge redistribution calculations on imidazole molecules further augments our finding that Im acts as a charge acceptor and HOPG acts as a charge donor.

Comparison of the density of states of isolated imidazole molecule and imidazole ligated to NiOEP on HOPG (Supporting Information, section E, Fig. SI-10) showed that lowest unoccupied band (consisting of s and p_z orbitals and lone pair of electrons on nitrogen, see dotted ovals in Figure SI-10) in isolated imidazole has moved to being part of the highest occupied band in Im-NiOEP/HOPG system. This result further corroborates imidazole as a charge acceptor from HOPG at the Im-NiOEP/HOPG interface. Additionally calculations show that work function (Table SI-5) of HOPG is reduced from 4.70 eV to 4.52 eV with NiOEP monolayer on HOPG. Our calculated work function for HOPG matches closely with experimental value. 64 Interestingly, ligation of imidazole to NiOEP further reduces the work function to 3.21 eV.

DFT calculations were able to establish the type of binding

interactions of imidazole to NiOEP on HOPG. The next step of the STM experiment is to determine if the imidazole ligation is dynamic at room temperature. Fig. 6 shows that successive scans over the same sample area containing both bright (circled) and dark molecules exhibit 'blinking', i.e. vanishing and appearance of the bright surface features. The appearance of new bright molecules after a 10 min scan delay is identified by blue circles in Fig. 5b. We interpret this behavior as evidence for the dynamic reversible ligation/de-ligation of Im from NiOEP/HOPG.

The ligation/de-ligation process can be monitored over prolonged periods of time and analyzed for possible equilibration. ^{27,54} A representative set of such measurements for the Im concentration of 1.5x10⁻³ M is plotted in Fig. 7. Here, the surface coverage (Θ), is defined as the number of bright molecules in an image (Im-NiOEP) divided by the total number of NiOEP surface molecules. The data in Fig. 7 were collected after the system had been allowed to come to equilibrium for 2 hours at 25 °C. The STM images analyzed contained about 225 surface NiOEP molecules and the average number of Im-NiOEP about 104 during the 30 min image collection period (for the Im concentration employed). Clearly there is exchange of Im occurring between the solution and the surface

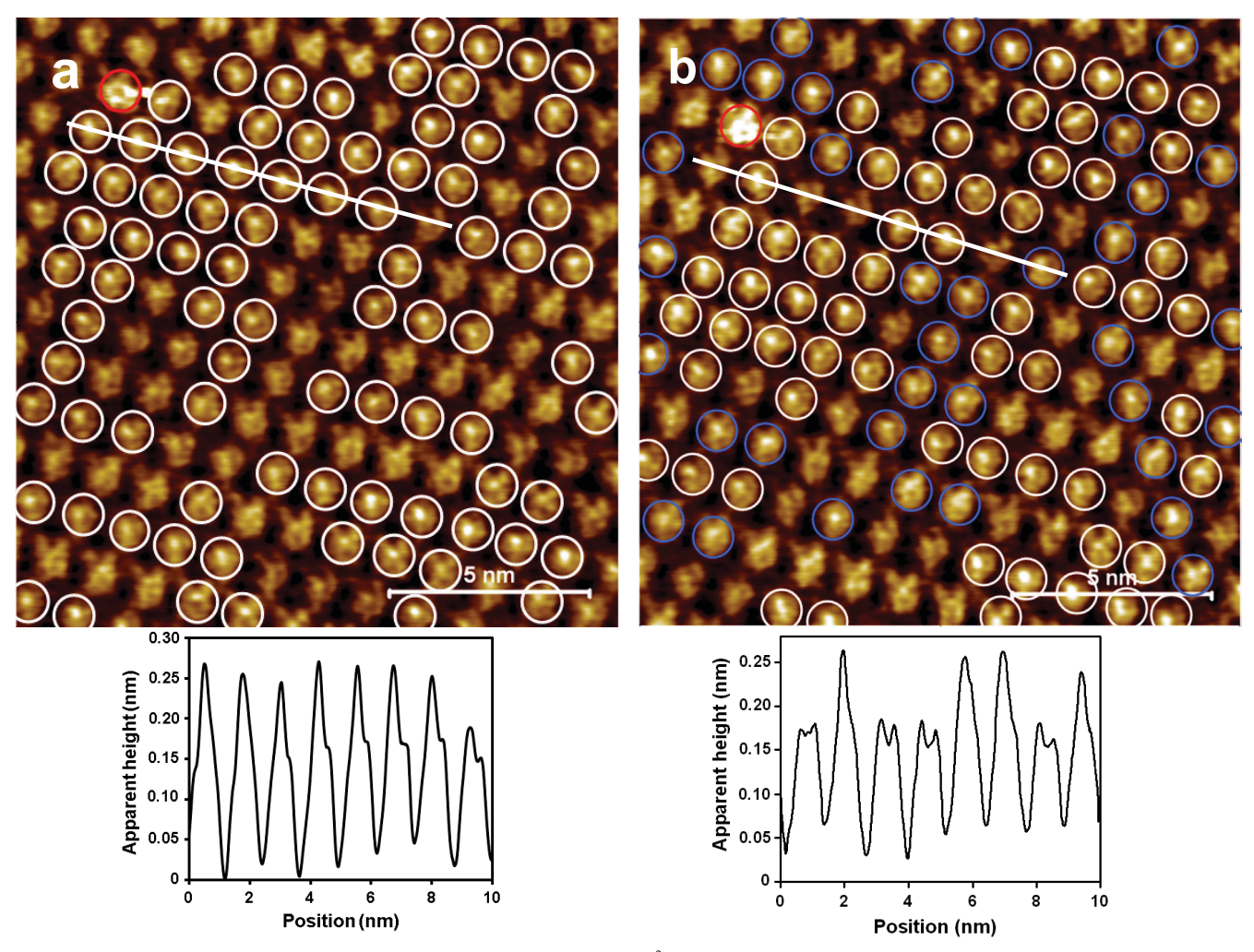


Fig. 6 Images of the 9NiOEP:1 H_2 OEP/HOPG surface in phenyloctane and Im (2.5x10⁻³ M in phenyloctane) collected after (a) addition of the ligand (defined as t = 0) and (b) 10 minutes later. Molecules circled in white and blue are coordinated to imidazole. The red circle denotes a marker. Below each image is a cross sectional profile. Although the location of the bound Im changes with time the average number of coordinated complexes is stationary –this demonstrates dynamic equilibration. Images were collected at 0.2 V and 50 pA set point.

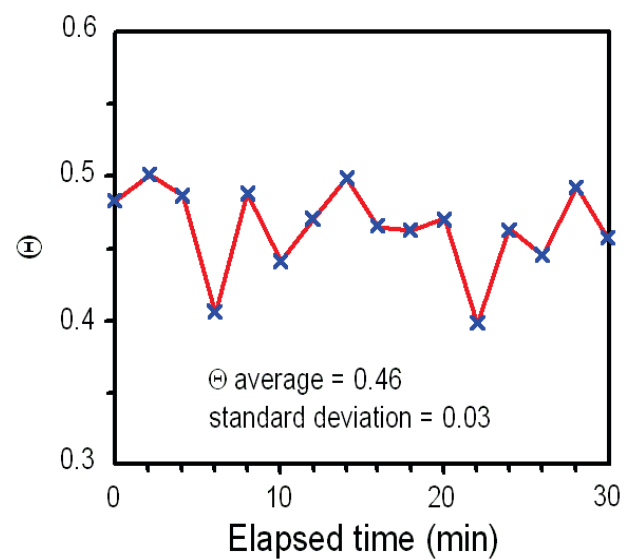


Fig. 7 Variation in Θ with time for $1.5x10^3$ M Im and 9:1 ratio of NiOEP to H_2OEP adsorbed on HOPG. STM scans were collected sequentially (2 min interval) over a period of 30 min at 25 °C.

supported NiOEP and the process has reached equilibrium.

Next we examined the binding affinity of the NiOEP/HOPG system toward Im as a function of ligand concentration. At least 5 separate binding experiments were conducted for each different Im solution concentration ranging from 2×10^{-4} M to 1.5×10^{-3} M. The same 9:1 molar mixture of NiOEP and H₂OEP was employed in all the Im concentration dependent binding studies. On the average 10-20 different images were collected for every binding experiment and the average surface coverage of Im-NiOEP complex was determined for each experiment. Following our earlier definition that Θ reflects the surface coverage of the Im–NiOEP complex, the quantity $\Theta/(1-\Theta)$ was plotted as a function of the solution concentration of the Im ligand (Fig. 8). The equilibrium process for Im binding to NiOEP clearly follows the Langmuir adsorption model which supposes a single binding energy and a maximum binding capacity corresponding to monolayer surface coverage.

The equilibrium constant, K_c, can be written as

$$K_{c} = \frac{\Theta}{(1-\Theta)(c/c^{0})}$$

where c⁰ is taken the solution standard state of 1 M Im and the

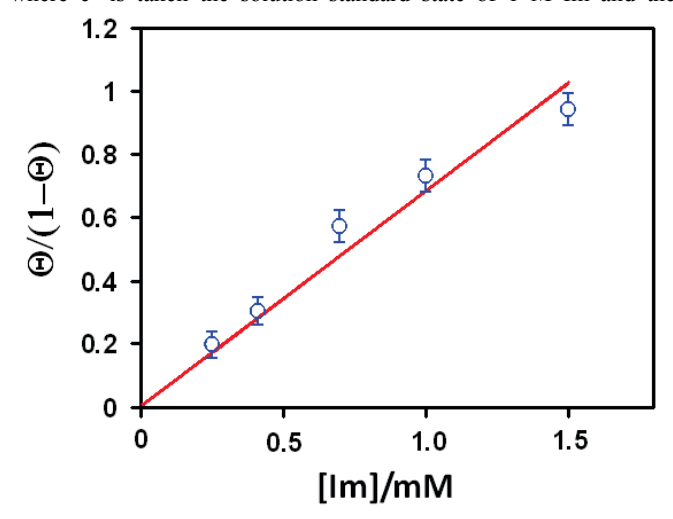


Fig. 8 The quantity $\Theta/(1-\Theta)$ as function of Im concentration employed is plotted using the Langmuir isotherm for the binding reaction at 25 °C. Standard deviations are also given. Θ is the fraction of NiOEP/HOPG bound to imidazole.

standard state coverage is 0.5. Using $\Delta G_c = -RT \ln(K_c)$, one can obtain the free energy for ligation of Im to NiOEP. From the plot in Fig. 8 we obtained K_c of 590 which gives a value of -15.8 kJ/mole for ΔG_c . The entropy (ΔS_c) associated with the formation of Im-NiOEP/HOPG is calculated to be -216 J/Kmol (see Supplemental Information, section F) using statistical mechanics. The value ΔH_c is then determined to be -80 kJ/mol. These values are comparable to the thermodynamic parameters obtained for the Im binding to metalloporphyrins in solution environments. Numerical variabilities may be ascribed primarily to differences in solubilities of the reactants in different solvents and to the active metals. 65, 66,67 Monoligation of a NiTMPyP(H2O) complex in an acetone-water mixture at 25°C lead to values of $\Delta H^{\circ} = -44.4 \text{ kJ/mole}$, $\Delta G^{\circ} = -5.2$ kJ/mol and $\Delta S^{\circ} = -131.4 \text{ J/K mol.}^{26}$ For the bis ligation reaction, of FeTPPCl + 2Im in acetone, $\Delta H^{\circ} = -83 \text{ kJ/mol}$, $\Delta S^{\circ} = -184 \text{ J/K mol}$, and $\Delta G^{\circ} = -27 \text{ kJ/mol.}^{67}$ The enthalpy for the addition of one imidazole ligand to Co(OCH₃)TPP in CH₂Cl₂ solvent was -59.6 kJ/mole, while ΔS° and ΔG° were -172.3 J/K mol and -8.3 kJ/ mol, respectively. 66 The axial ligation of imidazole and ZnTPP producing a five coordinated complex yielded $\Delta H^{\circ} = -157 \text{ kJ/mole}, \Delta G^{\circ} = -105$ kJ/mol, and $\Delta S^{\circ} = -173 J/K mol.^{65,68}$

Table 1 Summary of various quantitative properties obtained from PW-DFT calculations and STM experiments.

Property	Im-NiOEP ^a	NiOEP/HOPG ^a	Im-NiOEP/HOPG ^a	STM Experiment
Imidazole adsorption energy	-22 kJ/mol	-	-65 kJ/mol ^b	-80 kJ/mol
Porphyrin adsorption energy		2.30×10^2 kJ/mol		1.1± 0.1×10 ² kJ/mol ^c
Ground spin state	Triplet	Singlet	Singlet	
Charge distribution	NiOEP accepts 0.2 e-	HOPG accepts 0.1 e-	HOPG donates 0.4 e-	
Work function		4.52 eV	3.21 eV	

 $^{^{}a}$ PW-DFT calculated values; b Using PBE functional, with other functionals the energy range is $^{\sim}$ 33 to 65 kJ/mol. c Reference 54.

The STM data report a facile albeit weak (reversible) binding of imidazole to NiOEP in phenyloctane at the NiOEP/HOPG interface which can be readily interpreted in terms of charge contribution from HOPG, which acts as a ligand, bound to the fifth coordination site on the Ni ions. The 'five-coordinated' NiOEP receptors readily accept another ligand (Im) and form a six coordinated complex. In solution, of course, NiOEP does not bind Im. Our calculations also indicate that HOPG acts as an acceptor of electronic charge from NiOEP in the absence of imidazole but behaves as a donor in the presence of imidazole bound to NiOEP. In solution, Im is assumed to be primarily a two electron donating ligand binding to charge deficient Ni tetrapyrroles. 57,57 However, in the surface mediated scenario, the Im ligand acts as a π -acid while binding to NiOEP/HOPG. This unanticipated finding can be attributed to the ubiquitous nature of the imidazole ligand which can behave as a strong-field ligand (σ bonding) or as a π -donor or acceptor depending on the metal ion, the metal's oxidation state, and the nature of the other ligands present. Satterlee, based on NMR experiments, first suggested that imidazole-iron π -bonding is important in low-spin ferric porphyrin complexes, where imidazole acts primarily as a π -acceptor.²⁴ NiOEP adsorbed on HOPG surface binds Im in similar fashion, successfully imitating iron porphyrin receptors in biological systems.

The calculations further reveal that imidazole binds to the NiOEP adsorbate in a singlet ground state, an electronic condition not likely when NiOEP reacts with the ligand in the gas-phase or in solution. The HOPG substrate is then aiding the binding of Im to the NiOEP receptor by acting as a donor of charge while Ni ion retains S_0 state in the Im-NiOEP complex. This computational result is consistent with the transient nature of the imidazole nickel bond observed in the STM experiments.

Conclusions

It has been demonstrated that NiOEP binds imidazole reversibly at the solution/solid interface at 25 °C using STM imaging. NiOEP does not bind Im in solution. This is only the second reported study of a substrate directed ligand binding to a metalloporphyrin adsorbate imaged in a liquid environment. The first being the reversible O2 binding to CoOEP at the phenyloctane/HOPG interface. 13 The coordination of the ligand to the Ni ion in NiOEP adsorbed on HOPG as function of Im concentration was found to follow a simple Langmuir adsorption isotherm. The free energy for the binding reaction was small (-15.8 kJ/mole) and similar to ΔG values obtained for the Im binding to other metal porphyrins in solution environments. The reactivity of imidazole toward the NiOEP adsorbed on HOPG is attributed to charge donation from the graphite to the nickel ion (in a manner similar to an electrondonating ligand bound to the fifth coordination site) which stabilizes the Ni-Im bond.

Calculations revealed several unexpected characteristics about the NiOEP surface bound receptor and its coordination to imidazole: (1) Ni ion binds Im in a singlet ground state, (2) HOPG acts as an electronic charge acceptor from NiOEP without imidazole present but as a donor to the Im-NiOEP complex, and (3) Im acts as a π -acceptor when it binds to NiOEP/HOPG. These theoretical findings aided in explaining the STM data.

Our experimental and the theoretical results demonstrate that the reactivity of a metalloporphyrin receptor can be greatly influenced by the substrate and consequently have pronounced effects on the chemical sensing/recognition process. Practical utilization of organometallic complexes adsorbed on surfaces for sensing and catalysis warrants further studies. It will be important to investigate binding of other ligands to metalloporphyrins employing different solid supports (with different work functions and band structure) at the solution/solid interface. For example, ionic ligands may have different coordination affinity than neutral nitrogen bases toward porphyrin receptors bound to a surface.

Acknowledgements

This material is based upon work supported by the National Science Foundation under CHE-1403989. The computational work was performed using the Cascade super-computer from EMSL (proposal 48783), a DOE Office of Science User Facility sponsored by the Office of Biological and Environmental Research and located at Pacific Northwest National Laboratory (PNNL). Part of the computations was also supported by resources from the PNNL Institutional Computing (PIC) program at PNNL.

References

- J. Y. Liu, X. F. Li, Z. X. Guo, Y. Z. Li, A. J. Huang and W. B. Chang, J. Mol. Catal. A: Chemical., 2002, 179, 27–33.
- 2 A. Robertson and S. Shinkai, Coord. Chem. Rev., 2000, 205, 157–199.
- 3 K. M. Kadish, K. M. Smith and R. Guilard, Handbook of Porphyrin Science: With Applications to Chemistry, Physics, Materials Science, Engineering, Biology and Medicine. Catalysis and Bio-inspired systems. Volume 10, World Scientific. World Scientific Publishing Company (June 29, 2010) ISBN-10: 9814307181
- 4 M. F. Lucas, D. L. Rousseau and V. Guallar, *Biochim. Biophys. Acta* 2011, **1807**, 1305–1313.
- 5 K. M. Kadish, G. Rerriera, K. M. Smith and R. Guilard, Handbook of Porphyrin Science: With Applications to Chemistry, Physics, Materials Science, Engineering, Biology and Medicine. HemeBiochemistry. Volume 26, World Scientific. World Scientific Publishing Company (2013) ISBN-10: 981430718.
- 6 A. R. Smith and J. A. Klosek, Fuel Processing Technology 2001, 70, 115–134.
- 7 J. V. Barth, Nature Chemistry 2015, 7,105-120.
- 8 U. Mazur and K. W. Hipps, *Chem. Commun.* 2015, **51**, 4737 4749.
- 9 M. Li, D. den Boer, P. Iavicoli, J. Adisoejoso, H. Uji-I, M. Van der Auweraer, D. Amabilino, J. Elemans and S. De Feyter, *J. Am. Chem. Soc.*, 2014, **136**, 17418–17421.
- 10 D. den Boer, M. Li, T. Habets, P. Iavicoli, A. E. Rowan, R. J. M. Nolte, S. Speller, D. B. Amabilino, S. De Feyter and J. A. A. W. Elemans, *Nat. Chem.*, 2013, 5, 621–627.
- 11 J. M. Gottfried, Surf. Sci. Rep. 2015, 70, 259-379.

- 12 W. Auwärter, D. Ecija, F. Klappenberger, and J. V. Barth, *Nature Chem.* 2015, 7, 105-120.
- 13 B. A. Friesen, A. Bhattarai, K. W. Hipps and U. Mazur, J. Am. Chem. Soc., 2012, 134, 14897–14904.
- 14 A. Jahanbekam, B. Chilukuri, U. Mazur and K. W. Hipps, *J. Phys. Chem. C*, 2015, **119**, 25364–25376.
- 15 J. Visser, N. Katsonis, J. Vicario and B. L. Feringa, *Langmuir*, 2009, **25**, 5980–5985.
- 16 J. Otsuki, E. Seki, T. Taguchi, M. Asakawa and K. Miyake, Chemistry Letters, 2007, 36, 740-741.
- 17 Q. Ferreira, L. Alcacer and J. Morgado, *Nanotechnology*, 2011, **22**, 435604-435614.
- 18 R. Yerushalmi, D. Noy, K. K. Baldridge and A. Scherz, *J. Am. Chem. Soc.*, 2002, **124**, 8406-8415.
- 19 N. Shibayama, T. Inubushi, H. Morimoto and T. Yonetad, *Biochemistry*, 1987, **26**, 2194-2201.
- 20 K. M. Kadish, K. M. Smith and R. Guilard, *Handbook of Porphyrin Science* series., World Scientific Publishing Co., Hackensack, NJ. 2002-2016.
- 21 W. Macyk, A. Franke and G. Stochel, *Coord. Chem. Rev.*, 2005, **249**, 2437–2457.
- 22 S.-L. Jia, W. Jentzen, M. Shang, X.-Z. Song, J.-G. Ma, W. R. Scheidt and J. A. Shelnutt, *Inorg. Chem.*, 1998, **37**, 4402–4412.
- 23 W. K. Kaplan, R. A. Scott and K. S. Suslick, *J. Am. Chem. Soc.*, 1990, **112**, 1283-1285.
- 24 J. D. Satterlee, and G. N. La Mar, J. Am. Chem. Soc., 1976, 98, 2804–2808.
- 25 P. Bhyrappa, V. Krishnan, and M. Nethaji, *J. Chem. Soc. Dalton Trans.*, 1993, 1901-1906.
- 26 P. F. Pasternak, E. G. Spiro and M. Teach, *J. Inorg. Nucl. Chem.*, 1974, **36**, 599-606.
- 27 A. Bhattarai, U. Mazur and K. W. Hipps, J. Am. Chem. Soc., 2014, 136, 2142–2148.
- 28 SPIP; Image Metrology: Hørsholm, Denmark.
- 29 M.J. Frisch, et. al Gaussian 09, Revision A.1; Gaussian, Inc.: Wallingford, CT, 2009.
- 30 P. J. Stephens, F. J. Devlin, C. F. Chabalowski and M. J. Frisch, *J. Phys. Chem.* 1994, **98**, 11623-11627.
- 31 A. D. Becke, Phys. Rev. A, 1988, 38, 3098.
- 32 C. Lee, W. Yang and R.G. Parr, Phys. Rev. B, 1988, 37, 785.
- 33 R. Krishnan, J. S. Binkley, R. Seeger and J. A. Pople, *J. Chem. Phys.* 1980, **72**, 650–654.
- 34 A. V. Marenich, C. J. Cramer and D. G. Truhlar, *J. Phys. Chem. B*, 2009, **113**, 6378-6396.
- 35 J. P. Foster and F. Weinhold, *J. Am. Chem. Soc.* 1980, **102**, 7211-7218.
- 36 A. E. Reed, R. B. Weinstock and F. Weinhold, *J. Chem. Phys.* 1985, **83**, 735.
- 37 G. Kresse and J. Furthmüller, *Comput. Mater. Sci.* 1996, 6, 15–50.
- 38 G. Kresse and J. Furthmu"ller, *Phys. Rev. B: Condens. Matter Mater. Phys.*, 1996, **54**, 11169.
- 39 G. Kresse and J. Hafner, *Phys. Rev. B: Condens. Matter Mater. Phys.*, 1993, **47**, 558–561.
- 40 G. Kresse and D. Joubert, Phys. Rev. B: Condens. Matter Mater.

- Phys., 1999, 59, 1758.
- 41 P. E. Blöchl, *Phys. Rev. B: Condens. Matter Mater. Phys.*, 1994, **50**, 17953.
- 42 A. V. Krukau, O. A. Vydrov, A. F. Izmaylov and G. E. Scuseria, *J. Chem. Phys.*, 2006, **125**, 224106.
- 43 J. P. Perdew, K. Burke and M. Ernzerhof, *Phys. Rev. Lett.*, 1996, 77, 3865.
- 44 A. D. Becke, Phys. Rev. A, 1988, 38, 3098-3100.
- 45 M. Mura, A. Gulans, T. Thonhauser and L. Kantorovich, *Phys. Chem. Chem. Phys.*, 2010, **12**, 4759–4767.
- 46 B. Chilukuri, U. Mazur and K. W. Hipps, *Phys. Chem. Chem. Phys.* 2014, 16 14096-14107.
- 47 J. Klimeš, D. R. Bowler and A. Michaelides, *Phys. Rev. B: Condens. Matter Mater. Phys.*, 2011, **83**, 195131–195131.
- 48 J. Klimeš, D. R. Bowler and A. Michaelides, *J. Phys.: Condens. Matter*, 2010, **22**, 022201–5.
- 49 K. Lee, É. D. Murray, L. Kong, B. I. Lundqvist and D. C. Langreth, *Phys. Rev. B: Condens. Matter Mater. Phys.*, 2010, **82**, 081101–081104.
- 50 H. J. Monkhorst and J. D. Pack, *Phys. Rev. B: Solid State*, 1976, **13**, 5188-5192.
- 51 L. Scudiero, D. E. Barlow and K. W. Hipps, *J. Phys. Chem. B*, 2002, **106**, 996–1003.
- 52 Z. Q. Zou, L. Wei, F. Chen, Z. Liu, P. Thamyongkit, R. S. Loewe, J. S. Lindsey, U. Mohideen and D. F. Bocian, *J. Porph. Phthal.* 2005, **9**, 387-392
- 53 L. Scudiero and K. W. Hipps, *J. Phys. Chem. C*, 2007, **111**, 17516–17520.
- 54 A. Bhattarai, U. Mazur and K. W. Hipps, *J. Phys. Chem. C*, 2015, **119**, 9386–9394.
- 55 M. Dommaschk, C. Schütt, S. Venkataramani, U. Jana, C. Näther, F. D. Sönnichsen and R. Herges, *Dalton Trans.*, 2014, 43, 17395-17405.
- 56 D. Kim, Y. O. Su and T. G. Spiro, *Inorg. Chem.* 1986, 25, 3988-3993.
- 57 D. Noy, R. Yerushalmi, V. Brumfeld, I. Ashur, H. Scheer, K. K. Baldridge and A. Scherz, *J. Am. Chem. Soc.* 2000, **122**, 3937-3944
- 58 M. L. Shelby, M. W. Mara and L. X. Chen, Coord. Chem. Rev., 2014, 277–278, 291–299.
- 59 M. Mammen, E. J. Shakhnovich, J. M. Deutch and G. M. Whitesides, J. Org. Chem., 1998, 63, 3821–3830.
- 60 Y. Bai, F. Buchner, I. Kellner, M. Schmid, F. Vollnhals, H.-P. Steinrück, H. Marbach and J. M. Gottfried, New J. Phys., 2009, 11, 125004/1-125004/15.
- 61 W. Tang, E. Sanville and G. Henkelman, *J. Phys.: Condens. Matter*, 2009, **21**, 084204.
- 62 W. Song, N. Martsinovich, W. M. Heckl and M. Lackinger, *J. Am. Chem. Soc.*, 2013, **135**, 14854–14862.
- 63 B. Chilukuri and T. R. Cundari, Surf. Sci., 2012, 606, 1100– 1107.
- 64 CRC Handbook of Chemistry and Physics, 2008, pp. 12–114.
- 65 S. J. Cole, G. C. Curthoys, E. A. Magnusson and J. N. Phillips, *Inorg. Chem.*, **1972**, *11*, 1024-1028.
- 66 Z. Zhiang, V. Xi, Z. Zhihni, M. Gang, L. Huakuan and C.

- Rongi, Acta Physico Chimica Sinica, 1996, 12, 372-376.
- 67 P. R. Ciaccio, J. V. Ellis, M. E. Munson, G. L. Kedderis, F. X. McConville and J. M. Duclos, *J. Inorg, Nucl. Chem.*, 1976, 38, 1885-1889.
- 68 W. J. Ruan and Z. A. Zhu, Chinese J. Chem., 1999, 17, 438-447.